Inhibition of Hif1α prevents both trauma-induced and genetic heterotopic ossification

Shailesh Agarwal[a,1], Shawn Loder[a,1], Cameron Brownley[a], David Cholok[a], Laura Mangiavini[b], John Li[a], Christopher Breuler[a], Hsiao H. Sung[a], Shuli Li[a], Kavitha Ranganathan[a], Joshua Peterson[a], Ronald Tompkins[c], David Herndon[d], Wenzhong Xiao[e], Dolrudee Jumlongras[f], Bjorn R. Olsen[f], Thomas A. Davis[g], Yuji Mishina[h], Ernestina Schipani[b,2], and Benjamin Levi[a,2]

[a]Department of Surgery, University of Michigan, Ann Arbor, MI 48109; [b]Department of Orthopedic Surgery, University of Michigan, Ann Arbor, MI 48109; [c]Department of Surgery, Massachusetts General Hospital, Boston, MA 02114; [d]Department of Surgery, Shriners Hospital for Children and University of Texas Medical Branch, Galveston, TX 77555; [e]Department of Surgery, Genome Technology Center, Stanford University, Palo Alto, CA 94305; [f]Department of Developmental Biology, Harvard Dental School, Boston, MA 02115; [g]Regenerative Medicine Department, Naval Medical Research Center, Silver Spring, MD 20910; and [h]Department of Biologic and Materials Sciences, University of Michigan, Ann Arbor, MI 48109

Edited by Gregg L. Semenza, The Johns Hopkins University School of Medicine, Baltimore, MD, and approved December 4, 2015 (received for review August 4, 2015)

Pathologic extraskeletal bone formation, or heterotopic ossification (HO), occurs following mechanical trauma, burns, orthopedic operations, and in patients with hyperactivating mutations of the type I bone morphogenetic protein receptor *ACVR1* (Activin type 1 receptor). Extraskeletal bone forms through an endochondral process with a cartilage intermediary prompting the hypothesis that hypoxic signaling present during cartilage formation drives HO development and that HO precursor cells derive from a mesenchymal lineage as defined by *Paired related homeobox 1* (*Prx*). Here we demonstrate that Hypoxia inducible factor-1α (Hif1α), a key mediator of cellular adaptation to hypoxia, is highly expressed and active in three separate mouse models: trauma-induced, genetic, and a hybrid model of genetic and trauma-induced HO. In each of these models, Hif1α expression coincides with the expression of master transcription factor of cartilage, Sox9 [(sex determining region Y)-box 9]. Pharmacologic inhibition of Hif1α using PX-478 or rapamycin significantly decreased or inhibited extraskeletal bone formation. Importantly, de novo soft-tissue HO was eliminated or significantly diminished in treated mice. Lineage-tracing mice demonstrate that cells forming HO belong to the *Prx* lineage. Burn/tenotomy performed in lineage-specific Hif1α knockout mice (*Prx-Cre/Hif1α*$^{fl:fl}$) resulted in substantially decreased HO, and again lack of de novo soft-tissue HO. Genetic loss of *Hif1α* in mesenchymal cells marked by *Prx-cre* prevents the formation of the mesenchymal condensations as shown by routine histology and immunostaining for Sox9 and PDGFRα. Pharmacologic inhibition of Hif1α had a similar effect on mesenchymal condensation development. Our findings indicate that Hif1α represents a promising target to prevent *and* treat pathologic extraskeletal bone.

HIF1α | heterotopic ossification | cartilage | mesenchymal condensation | Prx

Heterotopic ossification (HO) is the pathologic formation of extraskeletal bone in soft tissues. This process occurs in two separate patient populations: those with severe trauma, including large surface-area burns, musculoskeletal injury, orthopedic operations, and even spinal cord injury; and those with a genetic disease known as fibrodysplasia ossificans progressiva (FOP) (1–4). FOP is caused by a hyperactivating mutation in the type I bone morphogenetic protein (BMP) receptor *ACVR1* (Activin type 1 receptor), and patients with FOP develop ectopic bone lesions in the absence of any substantial trauma. The clinical sequela of these pathologic ectopic bone formations, whether in the setting of trauma or genetic mutations, include nonhealing wounds, chronic pain, and joint immobility. In the case of FOP, progressive ossification may lead to death as a result of loss of thoracic cage compliance.

Treatment options for HO are limited because bone often recurs following surgical resection, and some patients may have nonresectable HO because of its sensitive location. The risk of an operation may outweigh the benefits of excision, especially in the face of recurrence (5). Therefore, there is a need to identify therapeutic options that can prevent HO before its initial occurrence in at-risk patients. Furthermore, the identification of a common treatment strategy for patients with musculoskeletal trauma and patients with FOP would represent a substantial advance in our understanding of these disease processes.

Several rodent models exist to study HO in the setting of musculoskeletal trauma or genetic mutation. In the burn/tenotomy model, mice undergo Achilles' tendon transection with concomitant partial-thickness dorsal burn injury; HO forms in this model at the tendon transection site (2, 3). To study genetic HO, two prominent models have evolved: (*i*) intramuscular HO through Ad.cre-inducible constitutively active *ACVR1* (*caACVR1: ACVR1 Q207D*) with cardiotoxin injection (1), and (*ii*) congenital HO in conditional *caACVR1* knockin mice [*Nfatc1* (nuclear factor of activated T-cells, cytoplasmic 1)-*cre*/*caACVR1*$^{fl/wt}$] (6). HO in the burn/tenotomy model and the *ACVR1*$^{fl/wt}$ models has been shown to develop through a cartilaginous intermediary, suggesting that this process occurs through endochondral ossification. Therefore, we hypothesized that targeting development of the cartilaginous intermediary would be sufficient to inhibit or minimize HO formation.

Significance

Heterotopic ossification (HO) is a debilitating condition in which bone forms inappropriately within soft tissues. Two vastly different patient populations are at risk for developing HO: those with musculoskeletal trauma or severe burns and those with a genetic mutation in the bone morphogenetic protein receptor *ACVR1* (Activin type 1 receptor). In this study, we demonstrate that both forms of HO share a common signaling pathway through hypoxia inducible factor-1α, and that pharmacologic inhibition or genetic knockout of this signaling pathway can mitigate and even abolish HO formation. These findings pave the way for pharmacologic inhibitors of hypoxia inducible factor-1α as therapeutic options for heterotopic ossification.

Author contributions: S.A., S. Loder, D.J., B.R.O., T.A.D., Y.M., E.S., and B.L. designed research; S.A., S. Loder, C. Brownley, D.C., L.M., J.L., H.H.S., K.R., J.P., R.T., D.H., W.X., B.R.O., and B.L. performed research; S.A., C. Breuler, H.H.S., S. Li, K.R., R.T., D.H., W.X., D.J., B.R.O., T.A.D., Y.M., E.S., and B.L. contributed new reagents/analytic tools; S.A., S. Loder, C. Brownley, D.C., L.M., J.L., C. Breuler, S. Li, J.P., D.H., W.X., B.R.O., T.A.D., Y.M., E.S., and B.L. analyzed data; and S.A., S. Loder, D.J., B.R.O., T.A.D., Y.M., E.S., and B.L. wrote the paper.

The authors declare no conflict of interest.

This article is a PNAS Direct Submission.

[1]S.A. and S. Loder contributed equally to this work.

[2]To whom correspondence may be addressed. Email: eschipan@med.umich.edu or blevi@umich.edu.

This article contains supporting information online at www.pnas.org/lookup/suppl/doi:10.1073/pnas.1515397113/-/DCSupplemental.

Hypoxia inducible factor-1α (Hif1α) is one particular signaling mediator that has been shown to be critical for normal chondrogenesis (7–10). Conditional Hif1α knockout mice have demonstrated that Hif1α is critical for chondrocyte survival and differentiation. Given the critical role of Hif1α in normal cartilage development and that HO forms through a cartilaginous intermediary, we hypothesized that targeting Hif1α through drug treatment or conditional Hif1α knockout would inhibit HO formation.

Results

Human Trauma Patients Exhibit Up-Regulation of HIF1α and Related Downstream Vascular Signaling Mediators. We used a genomic database of 244 patients at high risk for HO because of large surface-area burns to compare with unburned "control" patients (11, 12). A total of 25,000 genes were queried, of which 3,500 were noted to be significantly different in tissue from burn patients compared with control patients. A total of 25,000 genes were queried, of which 3,500 were noted to be significantly different in tissue from burn patients compared with control patients. In particular, we noted significant up-regulation of *HIF1α*, placing it within the top 50 up-regulated gene transcripts. In addition, related downstream gene transcripts, including *vWF* (von Willebrand factor), *PECAM* (platelet endothelial cell adhesion molecule-1), *FLT1* (fms-related tyrosine kinase 1), *CDH5* (cadherin 5), and *VEGF* were up-regulated (Fig. 1). In our evaluation of *HIF1α*, we queried the Ingenuity Pathway Knowledgebase for *HIF1α* downstream genes for which expression levels are previously known to be changed by activation of *HIF1α* (13, 14). The expression level of *HIF1α* was significantly up-regulated after burns [fold change = 2.103, false-discovery rate (FDR) < 0.05] with pathway activation *z*-score of 4.965, placing it within the top 50 up-regulated genes.

HO in Three Separate Animal Models Is Characterized by Elevated Hif1α Expression. Three separate models of HO were studied: (*i*) burn/tenotomy, (*ii*) Ad.cre/cardiotoxin-inducible caACVR1 expression, and (*iii*) congenital HO (*Nfatc1-cre/caACVR1*$^{fl/wt}$) (Fig. 2). Notably, when burn/tenotomy was performed in oxygen-dependent degradation domain (*ODD*)-*Luc* Hif1α reporter mice, we detected a highly positive signal at the tenotomy site compared with the uninjured side, which indicates that the tenotomy site becomes highly hypoxic (Fig. 3*A*). Immunostaining for Hif1α confirmed its expression in each of these three models (Fig. 3 *B–J*). Importantly, Hif1α was present during the precartilage and immature HO phases in the burn/tenotomy model and slowly receded with the formation of mature HO. In the burn/tenotomy model, Hif1α colocalized with the chondrogenic marker Sox9 [(sex determining region Y)-box 9], suggesting its intimate role in cartilage formation in this model (Fig. 3 *B–D*). Within mature HO observed 9 wk after trauma, Hif1α expression was present only within the marrow space of the heterotopic bone, but was no longer present within the osteoid or along the periphery of the HO lesion (Fig. 3*D*).

Similarly, HO lesions that developed in the Ad.cre/cardiotoxin model demonstrated a similar pattern of Hif1α expression with colocalization with Sox9 and pSmad 1/5, a known regulator of bone development (Fig. 3 *E–G*). Of note, inflammation is a common feature of both models, and therefore Hif1α stabilization is not an unexpected finding (13).

Therefore, to understand whether Hif1α plays a role in the formation of HO in the absence of inflammatory trauma, as in patients with hyperactive ACVR1, we used a model in which HO develops spontaneously as a result of constitutive activity of ACVR1 (*Nfatc1-Cre/caACVR1*$^{fl:wt}$) (14). These mice spontaneously develop HO lesions within 4–5 d after birth without

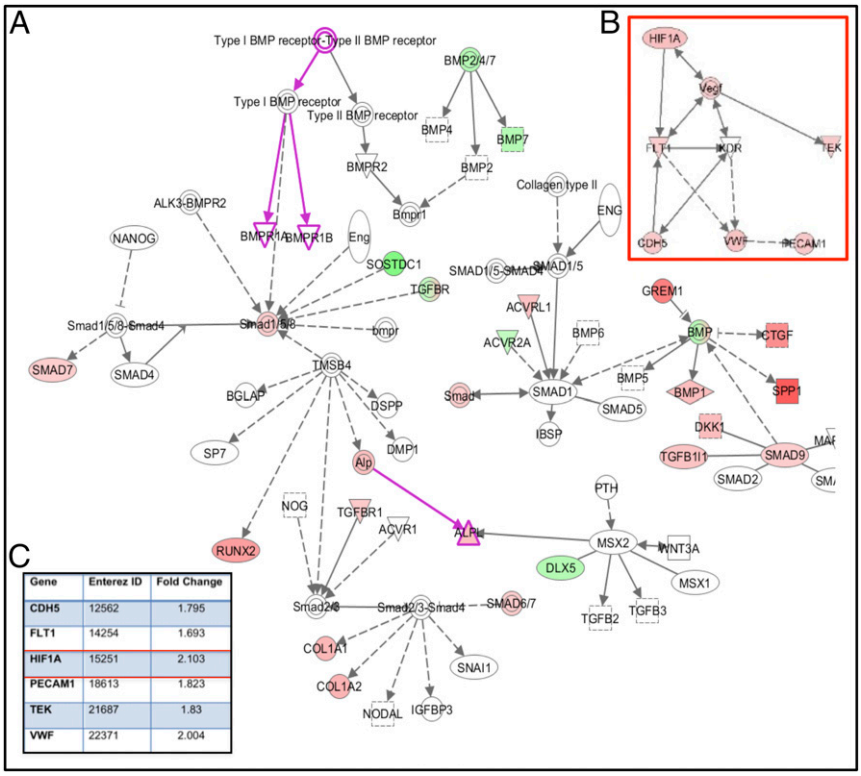

Gene	Enterez ID	Fold Change
CDH5	12562	1.795
FLT1	14254	1.693
HIF1A	15251	2.103
PECAM1	18613	1.823
TEK	21687	1.83
VWF	22371	2.004

Fig. 1. (*A*) Ingenuity pathway analysis of mRNA transcripts isolated from adipose tissue from burn or unburned "control" patients. (*B*) Up-regulation of the provasculogenic pathway, including *HIF1α*, *vWF*, *PECAM*, *FLT1*, *CDH5*, and *VEGF*. (*C*) Numeric-fold increase in gene expression of burn patients compared with unburned, control patients.

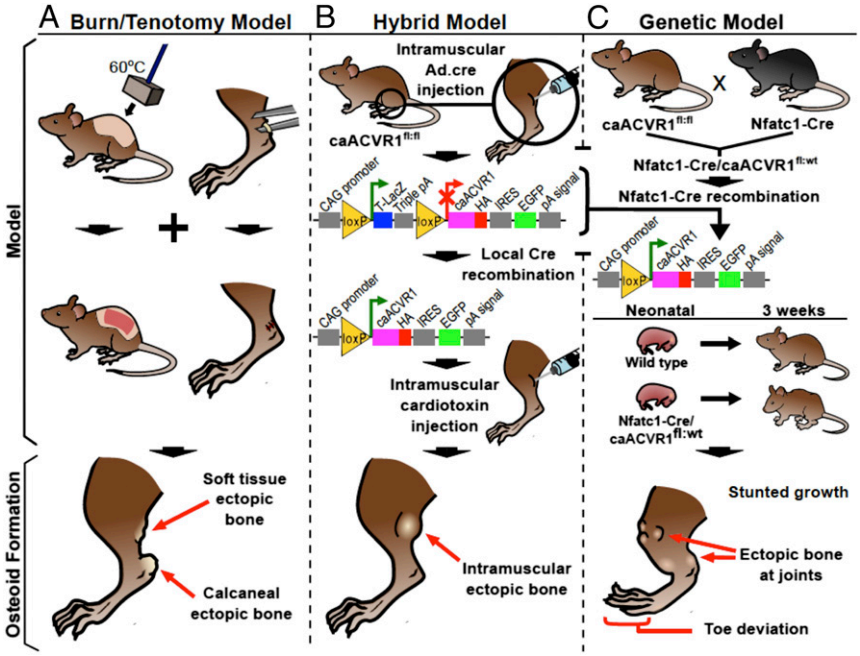

Fig. 2. (*A*) Trauma-induced model of HO in which mice receive a 30% total body surface-area partial-thickness dorsal burn injury with hindlimb Achilles' tendon transection, resulting in HO formation along the calcaneus as well as proximally within the soft tissue. (*B*) Hybrid model of HO wherein Ad.cre and cardiotoxin are injected into the gastrocnemius muscle of *caACVR1*$^{fl:fl}$ mice resulting in intramuscular HO formation. (*C*) *Nfatc1-Cre/caACVR1*$^{fl:wt}$ mice develop HO generally localized to the joints 4–5 d after birth in a model of genetic HO.

concomitant trauma or Ad.Cre or cardiotoxin injections. Lesions are generally localized to the joints, including ankles, knees, elbows, and digits (14). Immunostaining confirmed robust Hif1α expression within immature HO also in this model, which indicates that Hif1α plays a role in HO formation in the setting of hyperactive BMP receptor signaling despite absence of inflammatory trauma (Fig. 3 *H–J*). Again, robust colocalization of Hif1α with Sox9 and pSmad 1/5 was noted.

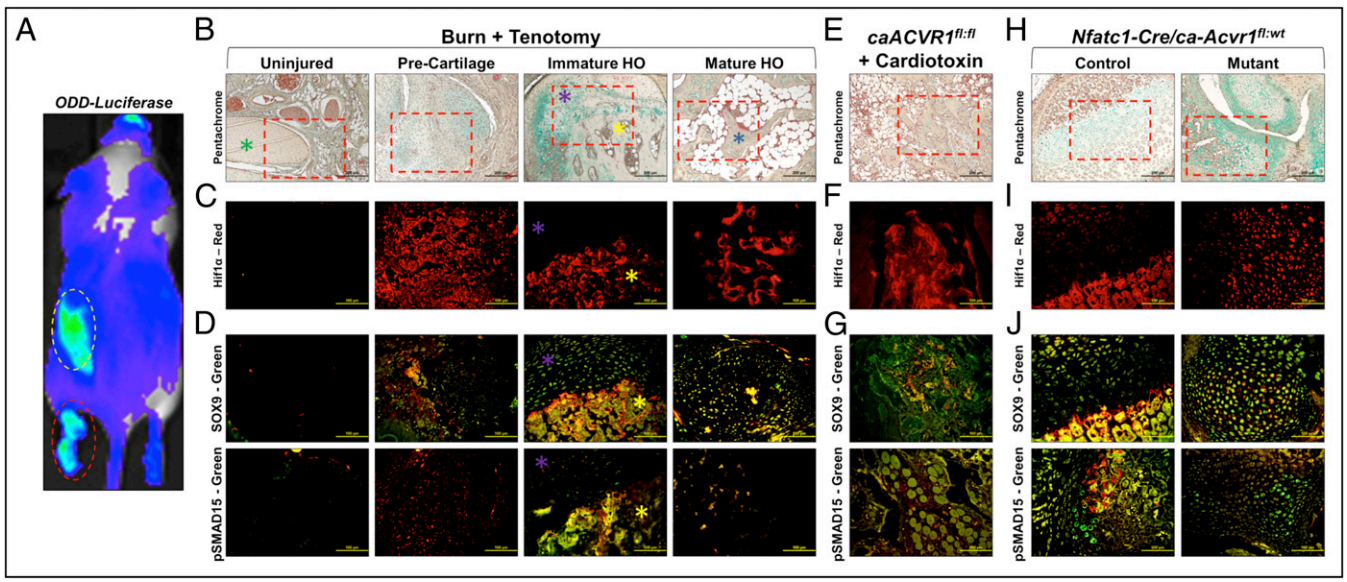

Fig. 3. (*A*) Bioluminescent image of Hif1α reporter *ODD-Luc* mouse after burn/tenotomy demonstrating increased signal at the burn (yellow circle) and tenotomy (red circle) sites. (*B*) Pentachrome images depicting uninjured hindlimb, and precartilage, cartilage anlagen with immature HO, and mature HO phases. (*C*) Immunostaining for Hif1α in uninjured, precartilage, immature HO, and mature HO showing robust expression in the precartilage and immature HO phases. (*D*) Costaining for Sox9 (green) or pSmad 1/5 (green) with Hif1α (red) in uninjured, precartilage, immature HO, and mature HO. (*E*) Pentachrome image of Ad.cre/cardiotoxin showing areas of cartilage and osteoid. (*F*) Immunostaining for Hif1α showing robust expression. (*G*) Costaining of Sox9 (green) or pSmad 1/5 (green) with Hif1α (red) in the Ad.cre/cardiotoxin model. (*H*) Pentachrome image of littermate control and *Nfatc1-cre/caACVR1*$^{fl/fl}$ mouse showing cartilage presence in the mutant. (*I*) Immunostaining for Hif1α showing robust expression within the mutant cartilage sites. (*J*) Costaining of Sox9 (green) or pSmad 1/5 (green) with Hif1α (red) in the *Nfatc1-cre/caACVR1*$^{fl/fl}$ mouse. Green asterisk, tendon; purple asterisk, cartilage anlagen; yellow asterisk, immature HO; blue asterisk, mature HO; white asterisk, native bone.

Taken together, these data show that Hif1α expression appears to be a common denominator in trauma-induced and genetic models of HO, and precedes cartilage formation and cartilage ossification, thereby validating it as a therapeutic target.

Pharmacologic Inhibition of Hif1α Limits HO After Burn/Tenotomy. Next, we tested the hypothesis that Hif1α inhibition can prevent HO. For this purpose, we used the drug PX-478, which has been shown to inhibit Hif1α transcription and translation (15). In vitro treatment of cells derived from the tenotomy site 3 weeks after injury (3WLST) and cultured in hypoxia showed diminished levels of the *Hif1α* transcript and of the chondrogenic gene transcripts *Sox9* and *Acan* (aggrecan) upon treatment with PX-478 (Fig. 4*A*). Additionally, PX-478 and rapamycin, a previously described Hif1α inhibitor (16), both significantly diminished Hif1α produced by mesenchymal cells isolated from tendon, confirming again that these drugs affect Hif1α levels in cells local to the future HO site (Fig. S1). We next tested whether treatment with PX-478 decreases Hif1α expression and cartilage formation in vivo, and consequently inhibits overall development of HO. Mice received burn/tenotomy and were subsequently treated with PX-478; histologic evaluation after 3 wk confirmed a substantial decrease in the cartilage anlagen, which is typically present after 3 wk (Fig. 4*B*). Furthermore, we found diminished Hif1α expression 3 wk after injury (Fig. 4*C*). Consistent with these data, expression of Sox9 was considerably diminished in the PX-478–treated group (Fig. 4*C*). Moreover, burn/tenotomy mice treated with PX-478 demonstrated a significant reduction in total HO volume at 5 wk (4.3 mm^3 vs. 1.5 mm^3, $P < 0.05$) and 9 wk (5.8 mm^3 vs. 2.3 mm^3, $P < 0.05$) after injury (Fig. 4 *D* and *E*). Finally, PX-478 treatment completely inhibited "soft tissue" HO—extraskeletal bone, which forms within the proximal transected tendon and distal gastrocnemius but away from the calcaneus—after 9 wk, as shown by binary analysis (yes/no: $\chi^2 = 9.5$, $P < 0.01$) and quantitative comparison (0.90 mm^3 vs. 0.00 mm^3, $P = 0.05$) (Fig. 4*E*). This result is notable, as soft tissue HO likely forms de novo without the influence of adjacent cartilage, bone, or periosteum normally located in close proximity to extraskeletal bone at the calcaneus. Taken together, these findings suggest that Hif1α is a permissive factor for chondrogenesis and its inhibition can prevent transition of nonosteochondro progenitor lineage cells into cells forming cartilage and ultimately extraskeletal bone. Notably, we found no adverse effects of PX-478 on wound healing of the burn or at the hindlimb tenotomy sites (Fig. S2). To test a second Hif1α inhibitor, mice were treated with rapamycin (16), resulting in significantly diminished de novo HO formation (1.60 mm^3 vs. 0.81 mm^3, $P < 0.05$) (Fig. 4 *F* and *G*) (16).

Pharmacologic Inhibition of Hif1α Limits HO Caused by ACVR1 Constitutive Activity. We next confirmed these findings in models of constitutive *ACVR1* activity caused by expression of the *caACVR1* (*ACVR1 Q207D*) mutation. ca$ACVR1^{fl/fl}$ mice injected with cardiotoxin and Ad.cre develop robust HO and this model has been used to study inhibitors of ACVR1 signaling. *caACVR1*$^{fl/fl}$ mice treated with PX-478 demonstrated near elimination of cartilage or bone based on pentachrome staining (Fig. 5*A*) after Ad.cre/cardiotoxin induction. Similarly, there was elimination of Hif1α and Sox9 based on immunostaining (Fig. 5*B*). Finally, microCT analysis confirmed the complete absence of HO in the PX-478 treated group based on binary analysis (yes/no; $\chi^2 = 13.6$, $P < 0.001$) and quantitative comparison (18.1 mm^3 vs. 0.01 mm^3, $P = 0.01$) (Fig. 5 *C* and *D*). These findings were striking because of the substantially improved efficacy over other BMP inhibitors in the literature. Pentachrome staining

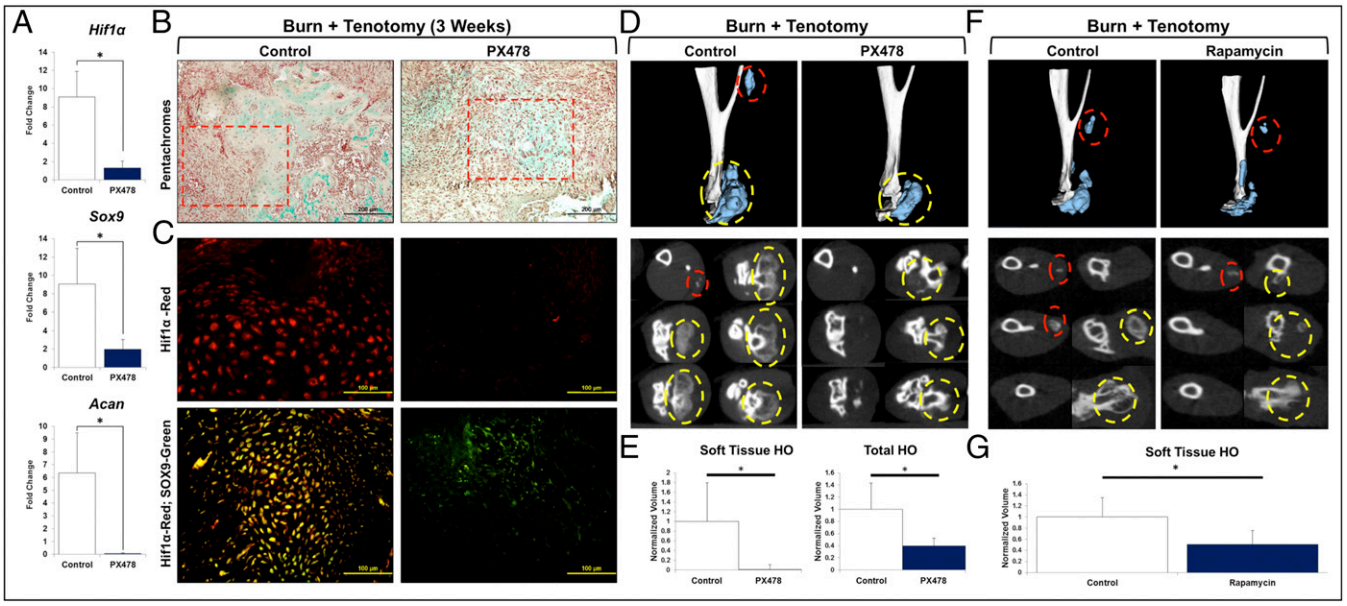

Fig. 4. (*A*) In vitro treatment of soft tissue cells isolated from tendon with PX-478 (10 μM) diminishes gene transcripts of *Hif1α*, *Sox9*, and *Acan* in chondrogenic differentiation medium. (*B*) PX-478 treatment of burn/tenotomy mouse substantially diminishes ossification and cartilage presence compared with control. (*C*) Immunostaining demonstrates substantially reduced Hif1α expression in PX-478–treated burn/tenotomy mice with concomitant reduction in Sox9 expression. (*D*) Three-dimensional reconstruction and serial cross-sections of microCT scans of PX-478 and control-treated burn/tenotomy mice. (*E*) PX-478 significantly decreases total HO volume in burn/tenotomy mice (5-wk volume: 4.3 mm^3 vs. 1.5 mm^3, $P < 0.05$; 9-wk volume: 5.8 mm^3 vs. 2.3 mm^3, $P < 0.05$; 9-wk normalized volume: 1.0 vs. 0.4, $P < 0.05$) and eliminates soft tissue HO in burn/tenotomy model (9-wk volume: 0.90 mm^3 vs. 0.00 mm^3, $P = 0.05$; 9-wk normalized volume: 1.0 vs. 0.0, $P = 0.05$; yes/no: $\chi^2 = 9.5$, $P < 0.01$). (*F*) Three-dimensional reconstruction and serial cross-sections of microCT scans of rapamycin and control-treated burn/tenotomy mice. (*G*) Rapamycin treatment significantly reduces de novo HO formation (9-wk volume: 1.60 mm^3 vs. 0.81 mm^3, $P < 0.05$; 9-wk normalized volume: 1.0 vs. 0.51, $P < 0.05$). *$P < 0.05$ for volumetric measurements; †$P < 0.05$ for binary analysis (yes/no); red circle, soft tissue heterotopic bone; yellow circle, calcaneal heterotopic bone; $n = 3$ for PX-478–treated mice; $n = 11$ for PX-478 control mice; $n = 5$ for rapamycin-treated mice; $n = 4$ for rapamycin control mice.

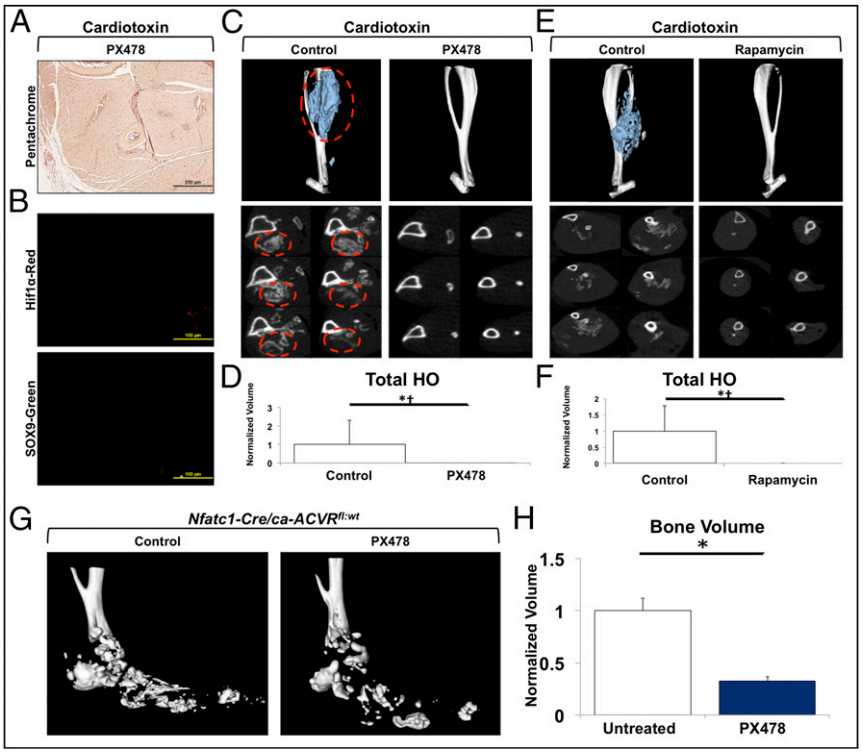

Fig. 5. (*A*) Pentachrome stain of Ad.cre/cardiotoxin-induced *caACVR1*$^{fl/fl}$ mouse treated with PX-478. (*B*) Absence of Hif1α or Sox9 expression after PX-478 treatment. (*C*) Three-dimensional reconstructions and cross-sections of microCT scans of PX-478 and control-treated hybrid model mice. (*D*) PX-478–treated hybrid model mice produced almost no evidence of HO on microCT compared with control-treated mice (control: $n = 12$ legs, PX-478: $n = 12$ legs) (volume: 18.1 mm^3 vs. 0.01 mm^3, $P = 0.01$; normalized volume: 1.0 vs. 0.0, $P = 0.01$; yes/no: $\chi^2 = 13.6$, $P < 0.001$). (*E*) Three-dimensional reconstructions and cross-sections of microCT scans of rapamycin and control-treated hybrid model mice. (*F*) Rapamycin-treated hybrid model mice produced no evidence of HO on microCT compared with control-treated mice (control: $n = 8$ legs, rapamycin: $n = 10$ legs) (volume: 17.5 mm^3 vs. 0.00 mm^3, $P < 0.001$; normalized volume: 1.0 vs. 0.0, $P < 0.05$; yes/no: $\chi^2 = 14.3$, $P < 0.001$). (*G*) Ankle reconstructions of control and PX-478–treated genetic HO mice. (*H*) Ankle extraskeletal bone volume quantification of genetic HO mice treated with control or PX-478 (800 Hounsfield units) (volume: 6.8 mm^3 vs. 2.2 mm^3, $P < 0.01$; normalized volume: 1.0 vs. 0.32, $P < 0.01$; $n = 4$ control treated legs; $n = 4$ PX-478–treated legs). *$P < 0.05$ for volumetric measurements; $^{\dagger}P < 0.05$ for binary analysis (yes/no); red circle, heterotopic bone.

confirmed absence of cartilage and bone (Fig. 5*C*) and immunostaining further confirmed absence of Hif1α and Sox9 expression (Fig. 5*D*). Again, these findings were replicated using rapamycin which showed complete absence of HO in treated mice (17.5 mm^3 vs. 0.0 mm^3, $P < 0.001$; yes/no; $\chi^2 = 14.3$, $P < 0.001$) (Fig. 5 *E* and *F*).

Finally, PX-478 was administered to mice with congenital HO (*Nfatc1-cre/caACVR1*$^{fl/fl}$) every other day starting from birth for 2 wk. Treated mice had significantly less ectopic bone at the ankle joints compared with mutant mice treated with vehicle (6.8 mm^3 vs. 2.2 mm^3, $P < 0.01$) (Fig. 5 *G* and *H*).

Genetic Loss of in Mesenchymal Progenitors Prevents Formation of Heterotopic Ossifications. To strengthen our findings, we next used a conditional *Hif1α* knockout mouse because global *Hif1α* knockout is embryonic lethal. We first established that heterotopic ossification following burn/tenotomy consists of cells from the *paired related homeobox* (*Prx*)-lineage using a series of lineage tracing experiments with *Prx-cre/ROSA26*^{mTmG} mice (Fig. 6). Importantly, we found that HO which formed within the soft tissue and more proximally within the soft tissue both exhibited nearly 100% presence of Prx-cre cells. In fact, we noted that the only non–Prx-cre cells present were those forming the marrow space of the mature HO.

We therefore used a mouse model of conditional *Hif1α* knockout in Prx-cre cells (*Prx-cre/Hif1α*$^{fl/fl}$). These mice have been shown to exhibit defective normal cartilage development (7). However, the impact on pathologic heterotopic ossification has not been demonstrated; therefore, burn/tenotomy was performed in *Prx-cre/Hif1α*$^{fl/fl}$ mice. Mutant mice developed minimal HO only around the calcaneus, and even these lesions were substantially smaller than in controls (5.02 mm^3 vs. 0.18 mm^3, $P < 0.01$) (Fig. 7 *A* and *B*).

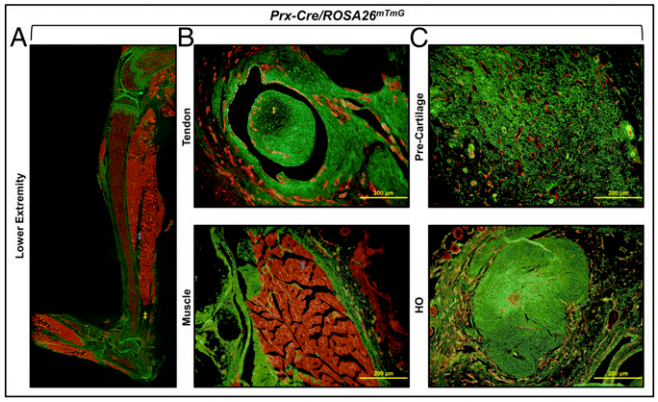

Fig. 6. (*A*) Longitudinal section of *Prx-cre/ROSA*^{mTmG} mouse hindlimb showing areas of Prx-cre cells (green). (*B*) Axial sections showing tendon and muscle of *Prx-cre/ROSA*^{mTmG} showing evidence of Prx-cre cells in tendon and connective tissue of muscle, but not within the myocytes. (*C*) Axial sections of precartilage and mature HO in *Prx-cre/ROSA*^{mTmG} showing that Prx-cre cells form the majority of HO.

Additionally, we noted that soft tissue HO was nearly completely abolished in mutant mice, consistent with our findings using PX-478 treatment based on volume (0.32 mm^3 vs. 0.01 mm^3) and binary analysis (yes/no; $\chi^2 = 3.7$, $P = 0.05$) (Fig. 7*B*).

Recognizing that the conditional *Hif1α* knockout mouse used in this study demonstrates growth plate abnormalities, we first evaluated the uninjured Achilles' tendon and tibia. The uninjured mutant tendon cross-sectional area was 60% of the littermate control, whereas the uninjured mutant tibial length was 32% of the littermate control. Importantly, the histologic appearance of the tendon appeared normal, as did the tibial cortex (Fig. 7*C*). Because of these differences in phenotype, we normalized HO values to either cross-sectional tendon area or tibial length (Fig. 7*D*). As expected, the differences remained significant because of the nearly complete absence of HO in the mutant model.

On histologic evaluation with serial pentachrome stains, we were unable to identify any regions of heterotopic ossification, either near the calcaneus or within the soft tissue (Fig. 7*E*). Therefore, histologic evaluation showed no evidence of cartilage presence, and nearly complete absence of Hif1α (Fig. 7*F*) and only minimal expression of Sox9 or pSmad 1/5 in mutant mice (Fig. 7*G*). These findings indicate that genetic loss of Hif1α in mesenchymal progenitor cells is sufficient to prevent formation of extraskeletal bone.

Loss of Hif1α Prevents Formation of Mesenchymal Condensations in HO Models. Next, we sought to understand why inhibiting Hif1α impairs HO formation. Therefore, the HO mesenchyme of conditional Hif1α knockout mice and littermate controls was evaluated 3 wk after burn/tenotomy injury. Routine histologic evaluation using H&E demonstrated absence of a mesenchymal condensation in the knockout mouse. Furthermore immunostaining for PDGFRα, a previously described marker of mesenchymal cells within mesenchymal condensations (17–19), and Sox9 confirmed the absence of mesenchymal condensation (Fig. 8 *A–C*). Similar to Hif1α knockout, PX-478 and rapamycin treatment substantially diminished the presence of mesenchymal progenitor cells and the formation of mesenchymal condensation as shown by H&E staining, as well as PDGFRα and Sox9 immunostaining (Fig. 8). We then searched for $PDGFR\alpha^+/Sox9^+$ cells in sites outside of the developing HO including the tendon-calcaneal insertion site of the uninjured hindlimb of treated or untreated mice, and Cre-conditional Hif1α knockout mice (Fig. S3). To confirm the effect of Hif1α inhibition on the Ad.cre/cardiotoxin model similar staining was performed for $PDGFR\alpha/Sox9^+$ cells. Again, we found a significantly diminished number of these cells in the setting of treatment 2 wk after induction (Fig. S4 *A* and *B*). To demonstrate a decrease in mesenchymal progenitor cells after early injury, we performed analyzed sections from the Ad.cre/cardiotoxin model 5 d after injury with similar results (Fig. S4*C*).

Discussion

HO is a pathologic process in two separate patient populations: those with severe burns and musculoskeletal trauma, and those with genetic mutations in the *ACVR1* gene conferring hyperactivity. To date, emphasis has been placed on the treatment of

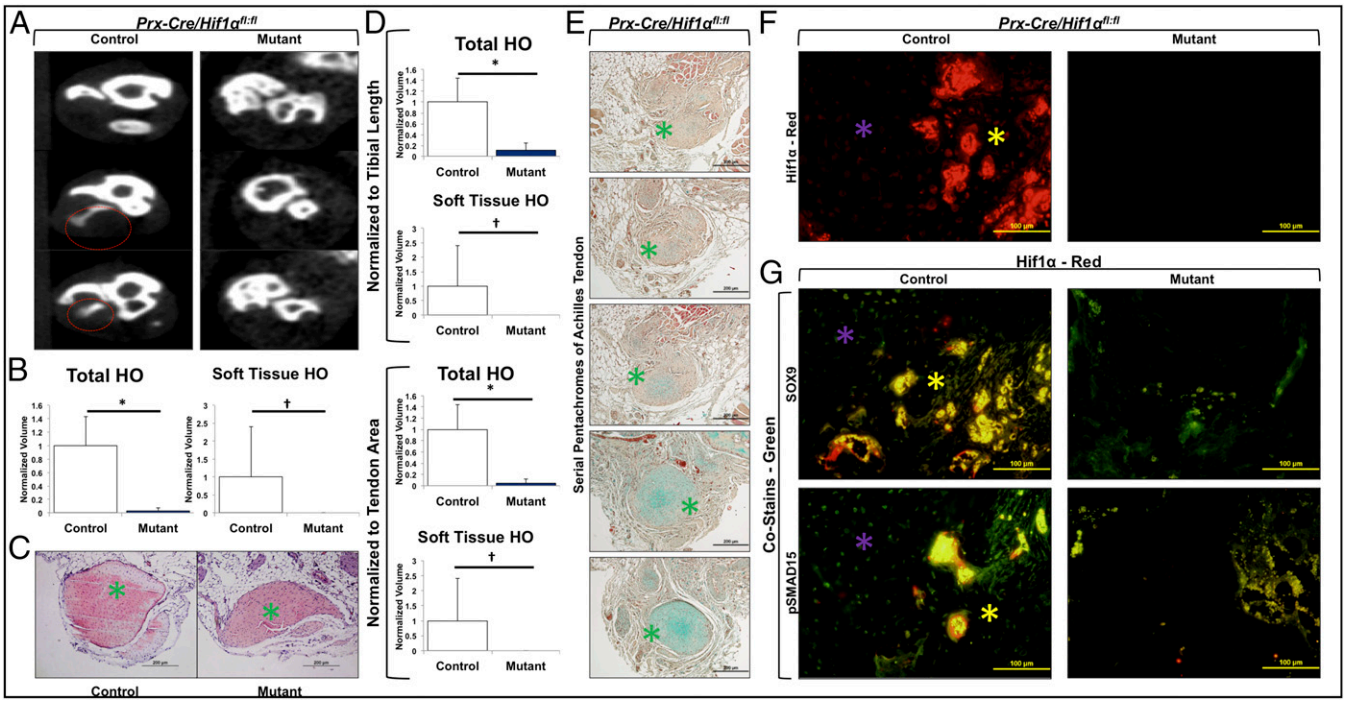

Fig. 7. (*A*) Serial microCT cross-sections showing *Prx-Cre/Hif1α*$^{fl:fl}$ mice make minimal total HO after burn/tenotomy and no soft tissue HO. (*B*) *Prx-Cre/Hif1α*$^{fl:fl}$ mice produce significantly less total HO (9-wk volume: 5.02 mm^3 vs. 0.18 mm^3, $P < 0.01$; 9-wk normalized volume: 1.0 vs. 0.03, $P < 0.01$) and soft tissue HO (9-wk volume: 0.32 mm^3 vs. 0.01 mm^3; 9-wk normalized volume: 1.0 vs. 0.0; yes/no: $\chi^2 = 3.7$, $P < 0.05$) compared with littermate controls. (*C*) Histologic image of representative tendon cross-sections in mutant and littermate control mice. (*D*) Total HO normalized to tibial length (total HO normalized to tibial length: 1.0 vs. 0.11, $P < 0.05$) or tendon cross-sectional area (total HO normalized to tendon cross-sectional area: 1.0 vs. 0.04, $P < 0.05$) and soft tissue HO normalized to tibial length (soft tissue HO normalized to tibial length: 1.0 vs. 0.0; yes/no: $P < 0.05$) or tendon cross-sectional area (soft tissue HO normalized to tendon cross-sectional area: 1.0 vs. 0.0; yes/no: $P < 0.05$). (*E*) Serial pentachrome images of *Prx-Cre/Hif1α*$^{fl:fl}$ 9 wk after burn/tenotomy confirming absence of ossification with minimal cartilage formation. (*F*) Absence of Hif1α expression after burn/tenotomy in mutant mice. (*G*) Corresponding absence of Sox9 (green) and pSmad 1/5 (green) expression after burn/tenotomy in mutant mice. *$P < 0.05$ for volumetric measurements; †$P < 0.05$ for binary analysis (yes/no); red circle, heterotopic bone; green asterisk, tendon; purple asterisk, cartilage anlagen; yellow asterisk, immature HO; $n = 4$ mutants; $n = 3$ littermate controls.

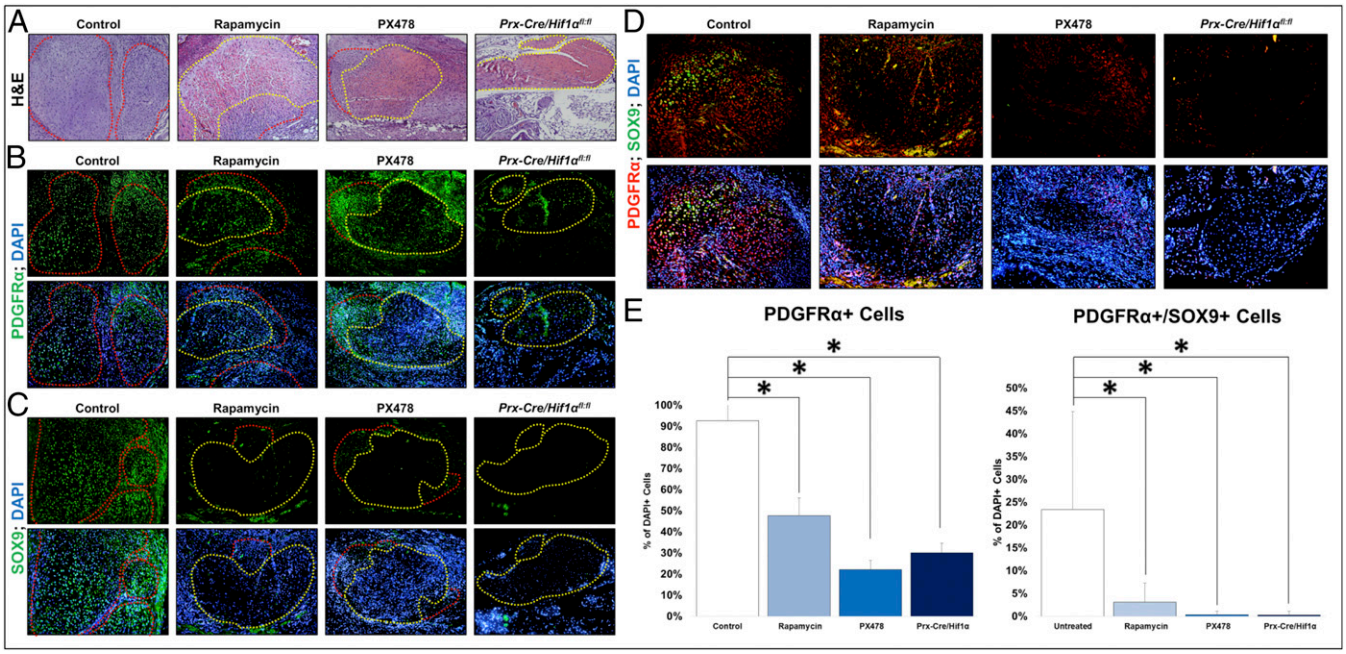

Fig. 8. (*A*) Absence of mesenchymal condensation based on H&E staining of *Hif1α* knockout mutant and diminished mesenchymal condensation in rapamycin- or PX-478–treated burn/tenotomy mice compared with control 3 wk after injury. (*B*) Absence of PDGFRα immunostaining in *Hif1α* knockout mutant and diminished PDGFRα immunostaining in rapamycin- or PX-478–treated burn/tenotomy mice compared with control 3 wk after injury. (*C*) Absence of Sox9 immunostaining in *Hif1α* knockout mutant and diminished Sox9 immunostaining in rapamycin- or PX-478–treated burn/tenotomy mice compared with control 3 wk after injury. (*D*) Absence of PDGFRα$^+$/Sox9$^+$ cells in *Hif1α* knockout mutant and diminished PDGFRα$^+$/Sox9$^+$ cells in rapamycin- or PX-478–treated burn/tenotomy mice compared with control 3 wk after injury. (*E*) Quantification of mesenchymal progenitor cells (PDGFRα$^+$) and condensing mesenchymal cells (PDGFRα$^+$/Sox9$^+$) cells. Yellow dotted line outlines tendon; red dotted line outlines mesenchymal condensation. *$P < 0.05$. (Magnification: 20×.)

patients with the *ACVR1* mutation, and a common signaling mediator between the two forms of HO has not been evaluated for therapeutic efficacy. Here, we leverage our knowledge of endochondral ossification to demonstrate that Hif1α represents a common target for both forms of ectopic bone formation. Genetic loss or pharmacologic inhibition of Hif1α significantly and consistently reduce or eliminate HO. Our findings are consistent in a model of trauma-induced HO with burn/tenotomy, and in two different models of genetic HO: one in which the constitutively active *ACVR1* gene is activated with exogenous Ad.cre injection and cardiotoxin to stimulate inflammation (*caACVR1*$^{fl/fl}$), and a second nontrauma model in which the constitutively active *ACVR1* gene is conditionally expressed from birth (*Nfatc1-cre*/*caACVR1*$^{fl/fl}$). These findings suggest that targeting the early phase of HO development—cartilage formation—represents a common solution to a pathology with several varying etiologies.

Transcriptome analysis shows significant up-regulation of Hif1α in adipose tissue isolated from burn patients. Mesenchymal cells with the capacity for osteogenic differentiation and which may serve as HO progenitor cells reside within adipose tissues, making this an appropriate tissue type to assay. Additionally, burn patients are a critical patient population at risk for trauma-induced HO development (2, 3, 20). Our recent analysis has shown that patients with burn total body surface area (TBSA) > 30% have 23-times higher odds of developing HO compared with patients with smaller surface-area burns, validating use of this cohort of patients with >20% TBSA burns for transcriptome analysis (21). Ingenuity pathway analysis showed that the Hif1α signaling pathway is up-regulated in the adipose tissues of burn patients, indicating downstream consequences. Although Hif1α is one of the top 50 transcription factors up-regulated in response to burn injury, other factors are also up-regulated. However, these initial findings prompted our interest in further evaluating Hif1α as it is highly expressed in response to trauma in tissues with mesenchymal cells capable of osteogenic differentiation, and is critical for cartilage development.

Histologic characterization of HO has established that, whether in the setting of trauma or mutated *ACVR1*, this process occurs through endochondral ossification. Endochondral ossification is characterized by the initial presence of mesenchymal cells, which condense and likely differentiate to form a cartilage template. Numerous studies have demonstrated that hypoxia induces chondrogenesis of mesenchymal cells, suggesting a prominent role for Hif1α. Additional data indicate that conditional loss of Hif1α within mesenchymal cells delays mesenchymal cell differentiation into chondrocytes (7).

Along these lines, in the setting of trauma-induced HO, the first step is a fibroproliferative stage that mimics the condensation event occurring during development. Both genetic loss of Hif1α in mesenchymal cells and pharmacologic inhibition of Hif1α severely impairs HO formation by preventing formation of mesenchymal condensations. In the model of conditional Hif1α knockout in Prx-cre cells, we found minimal HO formation with almost no mesenchymal condensations or cartilage formation. Previous gene knockdown efforts using siRNA suggest that Hif1α is important but are unable to account for the cells in which Hif1α signaling is critical. The *paired related homeobox* (*Prx* or *Prrx1*) lineage has previously been shown to mark the lateral plate mesoderm and limb bud mesenchyme (22). Using *Prx-cre*/*ROSA26*^{mTmG} mice, we showed that the Prx-cre$^+$ cells form HO throughout development from early chondrogenesis to late ossification. We therefore used this lineage to evaluate how genetic loss of Hif1α in this lineage affects HO using *Prx-cre*/*Hif1α*$^{fl/fl}$ mice. The absence of chondrogenesis following burn/tenotomy is consistent with studies demonstrating impaired growth plate formation in these mice. Based on the published data however, the complete absence of mesenchymal condensations

at the tendon transection site was unexpected but striking (7–9). Additionally, gene knockout reduced the number of mesenchymal progenitor cells, as determined by expression of PDGFRα. Treatment or gene knockout did not alter the presence of condensing mesenchymal cells in uninjured sites (e.g., tendon-calcaneal insertion or enthesis), as these cells are not present in the absence of injury. To confirm the absence of the mesenchymal condensations, we performed routine histologic evaluation with H&E in addition to immunostaining for PDGFRα (17–19) and Sox9 (7). Both PDGFRα and Sox9 have been previously described as markers of the developing mesenchyme, whereas H&E can also been used to identify the mesenchymal condensation (23).

In this study, we used two different drugs, PX-478 and rapamycin, to inhibit Hif1α (15, 16, 24–29). PX-478 has been shown to decrease Hif1α both in vitro and in vivo by decreasing *Hif1α* mRNA levels and blocking *Hif1α* mRNA translation (27, 30, 31). Constitutive VEGF signaling abrogates the effect of PX-478 on downstream angiogenic signaling, confirming that its effect is upstream of VEGF. Furthermore, the effect of PX-478 is limited to hypoxia, as angiogenic signaling is not altered in the presence of PX-478 under normoxic conditions (28). PX-478 does not appear to alter retinoic acid signaling, a pathway previously shown to affect HO formation (32). Separately, we used rapamycin, which inhibits Hif1α through the mammalian target of rapamycin (mTOR) (16, 33). When we tested these drugs in vitro on mesenchymal cells isolated from the tendon and cultured in hypoxia, we observed a significant decrease in Hif1α. Although both PX-478 and rapamycin may have off-target effects, their shared effect on Hif1α along with results from our conditional Hif1α knockout mouse indicate that pharmacologic inhibition of Hif1α is a viable therapeutic strategy to prevent HO. Similar to the effect of genetic loss, pharmacologic inhibition of Hif1α significantly diminished or eliminated de novo heterotopic bone, and diminished the number of mesenchymal progenitor cells and mesenchymal condensations.

Strikingly, in the setting of *ACVR1* mutation, pharmacologic Hif1α inhibition with PX-478 or rapamycin again prevents HO formation. This finding suggests that constitutive ACVR1 activity alone is not sufficient to induce HO, and is consistent with our clinical knowledge that patients with fibrodysplasia ossificans progressiva who have a hyperactivating mutation in *ACVR1* (*ACVR1 R206H*) develop ectopic bone lesions following minor trauma (4). Similar to the burn/tenotomy model, we found that mesenchymal cells marked by coexpression of PDGFRα and Sox9 were present in the developing lesion of untreated mice, but eliminated in the setting of therapeutic Hif1α inhibition. The effect of PX-478 on heterotopic bone in the *Nfatc1-cre* model is consistent with the role of Hif1α in cartilage maintenance, as previously reported (9, 12). To our knowledge, for the first time a common target has been demonstrated between trauma-induced and genetic HO that is consistent with the developmental role of Hif1α in endochondral ossification. These findings also suggest that pharmacologic agents with Hif1α inhibitory potential, such as PX-478 or rapamycin, may serve as therapeutic options even for HO caused by hyperactive *ACVR1* signaling. Previously, siRNA directed against Hif1α has been shown to decrease HO formation in a burn/tenotomy model (34). Our study develops these preliminary findings by demonstrating that available pharmacologic agents deserve attention for inhibitory potential in patients. siRNA currently lacks therapeutic efficacy in patients with heterotopic ossification, prompting the need for therapeutic options such as PX-478 or rapamycin. It is nearly impossible to determine the exact anatomic location where HO will form, making it difficult to precisely deliver local treatments. This challenge associated with local delivery can be obviated with systemic delivery of pharmacologic options. However, we acknowledge that further studies must be performed to determine the optimal dosing and timing of administration of these drugs.

Our findings suggest a new paradigm for treatment of heterotopic ossifications that targets Hif1α. We found that pharmacotherapy with Hif1α inhibitors, such as rapamycin or PX-478, can potently diminish extraskeletal bone formation in different models of HO. This effect appears to be related to diminution or absence of mesenchymal condensations which precede HO formation.

Methods

Ethics Statement. All animal experiments described were approved by the University Committee on Use and Care of Animals at the University of Michigan, Ann Arbor (Protocols: #05909, 05182, and 05716). This study was carried out in strict accordance with the recommendations in the *Guide for the Care and Use of Laboratory Animals of the National Institutes of Health* (35). All animal procedures were carried out in accordance with the guidelines provided in the *Guide for the Use and Care of Laboratory Animals: Eighth Edition* from the Institute for Laboratory Animal Research (35). Institutional review board approval was obtained through the University of Michigan (HUM051190), University of Texas Medical Branch, University of Florida, and Massachusetts General Hospital.

Patient Enrollment and Sampling for Gene-Expression Profiling. Written consent was obtained for all human studies. Institutional review board approval was obtained through the University of Texas Medical Branch. Patient enrollment and sample collection for patients have been described previously (36). Between 2000 and 2009, 244 burn patients were enrolled at one of four burn centers if admission occurred within 96 h postinjury, at least 20% of the TBSA was affected, and at least one excision and grafting procedure was required. Additionally, 35 healthy control subjects (16–55 y) were recruited between 2004 and 2007. In both the burn patients and the control patients, adipose tissue was collected and analyzed for RNA transcript levels. Using a fine scissor or scalpel, 80 mg of adipose tissue was obtained and immediately placed on an iced Petri dish and cut into a 2- to 5-mm cube. The sample was placed in a cryogenic tube containing 2 mL RNAlater to stabilize the tissue according to standard operating procedure B001.03, and the tissue was processed to total cellular RNA using a commercial RNA purification kit (RNeasy, Qiagen) according to standard operating procedure G026.01. Biotinylated cRNA was generated from 4 μg of total cellular RNA, hybridized onto HU133 Plus 2.0 GeneChips, stained, and washed according to the manufacturer's recommendations. A total of 25,000 genes were queried, of which 3,500 were significantly changed with an FDR < 0.001 and defined fold-change ≥ 1.5.

Analysis of Time-Course Gene-Expression Data. Specimens were immediately stabilized using RNAlater (Ambion). Total cellular RNA was extracted from the remaining specimens with good quality using a commercial RNA purification kit (RNeasy, Qiagen). Biotinylated cRNA was generated from 1 μg of total cellular RNA using the 3′ IVT Express Kit and protocol of Affymetrix, and hybridized onto an HU133 Plus 2.0 GeneChip (Affymetrix). EDGE (Extraction of Differential Gene Expression) was used to estimate the significance of expression changes for each gene by 1,000 random permutations. Significant genes were selected by FDR < 0.001 and fold-change ≥ 1.5. These genes were further analyzed using ingenuity pathway analysis (37).

Animals. Mice included for extraskeletal bone evaluation were wild-type C57BL/6 (Charles River Laboratory), *Cdh5-Cre/tdTomato*$^{fl/wt}$, *Prx-Cre/Hif1α*$^{fl/fl}$, *Prx-Cre/ROSA26*^{mTmG}, *caAcvr1*$^{fl/fl}$, *Nfatc1-Cre/caAcvr1*$^{fl/wt}$, or littermate controls. All breeding was performed at the University of Michigan in facilities managed by the Unit for Laboratory Animal Medicine at the University of Michigan. Tail genomic DNA was used for genotyping. Mice used for bioluminescent imaging were homozygous for the *ODD-luc* transgene. In these mice, the C-terminal portion of the hip1α ODD is fused to the firefly luciferase (*luc*) gene. Hypoxia causes stabilization of the fusion protein thereby increasing fluorescence upon luciferin administration.

Extraskeletal Bone Models. All mice received presurgical analgesia consisting of 0.1 mg/kg buprenorphine, followed by anesthesia with inhaled isoflurane, and close postoperative monitoring with analgesic administration.

Burn/tenotomy mice received a 30% TBSA partial-thickness burn on the shaved dorsum followed by left hindlimb Achilles' tendon transection. The dorsum was burned using a metal block heated to 60 °C in a water bath and applied to the dorsum for 18 s continuously. The tenotomy site was closed with a single 5-0 vicryl stitch placed through the skin only.

caAcvr1$^{fl:fl}$ mice received hindlimb cardiotoxin and Ad.cre injection at postnatal day 24. Mice were then killed after 22 d (PX-478) or 15 d (rapamycin).

Separate controls were used for each drug treatment to account for differences in the day of killing.

Nfatc1-Cre/caAcvr1$^{fl:wt}$ mice were generated by crossing *Nfatc1-Cre*$^{+}$ mice with *caAcvr1*$^{fl:wt}$ mice. Resulting mutants developed extraskeletal bone by postnatal day 4–5.

Drug Treatment. Burn/tenotomy or hybrid HO mice were administered PX-478 (100 mg/kg) or rapamycin (5 mg/kg) in PBS solution via intraperitoneal injection. Mice received injections every other day for the duration of the study. *Nfatc1-Cre/caACVR1*$^{fl:wt}$ mice were administered PX-478 (100 mg/kg) every other day for a total of 2 wk.

Isolation and Culture of Mesenchymal Stem Cells. Mouse mesenchymal stem cells were harvested from the tendon transection site originating from the calcaneus to the confluence of the fibula and tibia in wild-type mice. All tissue was mechanically minced and digested with collagenase A and dispase, and subsequently plated. To test drug treatment on Hif1α expression, cells were cultured in a hypoxia chamber with 0.5% oxygen. Cell treatment with PX-478 (10 μM) or rapamycin (5 μM) was initiated 24 h before hypoxia treatment and redosed in hypoxia for 24 h. Protein was harvested and analyzed using Western blot for Hif1α and α-tubulin. To test effect of PX-478 treatment on chondrogenesis, cells isolated from the tendon were cultured in chondrogenic differentiation medium (PT-3925 and PT-4121; Lonza). All in vitro experiments were performed in biologic and technical triplicate.

Histology and Immunofluorescence. Histologic evaluation was performed at indicated time points in burn/tenotomy, Ad.cre/cardiotoxin, or *Nfatc1-Cre/caAcvr1*$^{fl:wt}$ mutants. Hind limbs were fixed in formalin overnight at 4 °C and subsequently decalcified in 19% (mass/vol) EDTA solution for 3–5 wk at 4 °C until X-ray verification of decalcification. Hind limbs were paraffin- or cryo-embedded, and 5- to 7-μm sections were cut and mounted on Superfrost plus slides (Fisher) and stored at room temperature. H&E and Movat's pentachrome staining were performed of the ankle region. Immunostaining staining of extraskeletal ectopic bone was performed on rehydrated wax sections with the following primary antibodies: mouse anti-mouse anti-Hif1α (Santa Cruz, Cat No. 53546), goat anti-mouse anti-Cdh5 (Santa Cruz, Cat No. 6458), goat anti-mouse anti-pSmad 1/5 (Santa Cruz, Cat No. 12353), goat anti-mouse anti-CD31 (Santa Cruz, Cat No. 1506), rabbit anti-mouse anti-Sox9 (Santa Cruz, Cat No. 20095), or anti-mouse PDGFRα. Appropriate dilutions were determined before achieving final images. The appropriate fluorescent secondary antibody was applied and visualized using fluorescent microscopy. Secondary antibodies consisted of anti-rabbit or anti-goat Alexafluor-488 (green) or -594 (red). All mouse sections were taken 3 wk after burn/tenotomy. All counts were performed by blinded observer with 15 high-power fields for each sample.

Fluorescent and Bioluminescent Imaging. All fluorescent and bioluminescent imaging was acquired using a PerkinElmer IVIS Spectrum system. Wild-type C57BL/6 mice were used for fluorescent imaging to assess vascular perfusion. Mice were administered Angiosense 750 EX via tail vein injection. Fluorescent imaging was acquired 24 h after injection at 770-nm wavelength. *ODD-luc* were used for all bioluminescent imaging. Mice received luciferin intraperitoneal injection ten minutes before imaging.

Quantitative PCR. Tissue was harvested from the tenotomy site of burn/tenotomy mice, or from the corresponding contralateral, control hindlimb at indicated time points. RNA was collected from tissue using RNeasy Mini Kit (Qiagen) according to the manufacturer's specifications. Reverse transcription was performed with 1 μg RNA using Taqman Reverse Transcription Reagents (Applied Biosystems). Quantitative real-time PCR was carried out using the Applied Biosystems Prism 7900HT Sequence Detection System and Sybr Green PCR Master Mix (Applied Biosystems). Specific primers for these genes were chosen based on their PrimerBank sequence (Table S1).

MicroCT and Nano-CT Analysis. MicroCT scans (Siemens Inveon using 80-kVp, 80-mA, and 1,100-ms exposure) were used to quantify extraskeletal bone growth in burn/tenotomy, Ad.cre/cardiotoxin, or mutant *Nfatc1-cre/caAcvr1*$^{fl:wt}$ mice. Burn/tenotomy mice received scans at 5 and 9 wk after tenotomy. Ad.cre/cardiotoxin mice received microCT scans at day 22 after induction with Ad.cre and cardiotoxin injection. *Nfatc1-cre/caAcvr1*$^{fl:wt}$ mice and littermate controls received microCT scansat day 13 after birth. Images were reconstructed and HO volume quantified using a calibrated imaging protocol as previously described with the MicroView microCT viewer (Parallax Innovations).

Microscopy. All fluorescently stained images were taken using an Olympus BX-51 upright light microscope equipped with standard DAPI, 488 nm, and TRITC cubes attached to an Olympus DP-70 high-resolution digital camera. Each site was imaged in all channels and overlaid in DPViewer before examination in Adobe Photoshop.

Statistical Analysis. A power analysis was first performed to determine how many mice were needed for our PX-478 treatment groups. For power analysis, the primary outcome of interest is differences in HO volume with treatment. To confirm a 50% decrease in HO volume with power of 0.8, assuming an SD of 1.5 mm^3 and mean HO volume of 7.5 mm^3 in untreated mice, we required three mice per group. Means and SDs were calculated from numerical data, as presented in the text, figures, and figure legends. In figures, bar graphs represent means, whereas error bars represent one SD. Statistical analysis was performed using an appropriate analysis of variance when more than two groups were compared, followed by a post hoc Student's *t* test (with a Bonferroni correction) to directly compare two groups. Inequality of SDs was excluded by using the Levene's test. Outliers were excluded using the Grubb's test for outliers. *P* values are included in the figure legends.

ACKNOWLEDGMENTS. We thank the Department of Radiology at The University of Michigan for the use of The Center for Molecular Imaging and the Tumor Imaging Core which are supported in part by NIH Grant P30 CA046592. This work was supported in part by a Coller Society Research Fellowship (to S.A.); National Institutes of Health (NIH) Loan Repayment Program (S.A.); the Plastic Surgery Foundation (S.A.); NIH F32 Fellowship (to S.A. and K.R.); the Howard Hughes Medical Institute Medical Fellows Program (S. Loder); NIH Grant R01 DE020843 (to Y.M.); Department of Defense Grant W81XWH-11-2-0073 (to Y.M.); NIH Grant U54GM062119 (to R.T.); NIH Grants R01 AR036820 and P01 AR048564 (to B.R.O.); and NIH National Institute of Arthritis and Musculoskeletal and Skin Diseases Grant R01AR065403-02 (to E.S.). B.L. received funding from NIH/National Institute of General Medical Sciences Grant K08GM109105-0, Plastic Surgery Foundation National Endowment Award, the Association for Academic Surgery Roslyn Award, American Association for the Surgery of Trauma Research & Education Foundation Scholarship, DOD: W81XWH-14-DMRDP-CRMRP-NMSIRA and American Association of Plastic Surgery Research Fellowship. Some of the authors are employees of the United States Government. This work was prepared as part of their official duties. Title 17 U.S.C. §105 provides that "Copyright protection under this title is not available for any work of the United States Government." Title 17 U.S.C §101 defined a US Government work as a work prepared by a military service member or employees of the United States Government as part of that person's official duties. The opinions or assertions contained in this paper are the private views of the authors and are not to be construed as reflecting the views, policy or positions of the Department of the Navy, Department of Defense nor the United States Government. This work was partially supported by DOD work units W81XWH-14-2-0010 and 602115HP.3720.001.A1014.

1. Yu PB, et al. (2008) BMP type I receptor inhibition reduces heterotopic [corrected] ossification. *Nat Med* 14(12):1363–1369.
2. Peterson JR, et al. (2014) Treatment of heterotopic ossification through remote ATP hydrolysis. *Sci Transl Med* 6(255):255ra132.
3. Peterson JR, et al. (2014) Burn injury enhances bone formation in heterotopic ossification model. *Ann Surg* 259(5):993–998.
4. Shore EM, et al. (2006) A recurrent mutation in the BMP type I receptor ACVR1 causes inherited and sporadic fibrodysplasia ossificans progressiva. *Nat Genet* 38(5):525–527.
5. Pavey GJ, et al. (2015) What risk factors predict recurrence of heterotopic ossification after excision in combat-related amputations? *Clin Orthop Relat Res* 473(9): 2814–2824.
6. Asai S, et al. (2014) Tendon progenitor cells in injured tendons have strong chondrogenic potential: the CD105-negative subpopulation induces chondrogenic degeneration. *Stem Cells* 32(12):3266–3277.
7. Provot S, et al. (2007) Hif-1alpha regulates differentiation of limb bud mesenchyme and joint development. *J Cell Biol* 177(3):451–464.
8. Schipani E (2006) Hypoxia and HIF-1alpha in chondrogenesis. *Ann N Y Acad Sci* 1068:66–73.
9. Schipani E, et al. (2001) Hypoxia in cartilage: HIF-1alpha is essential for chondrocyte growth arrest and survival. *Genes Dev* 15(21):2865–2876.
10. Wang Y, et al. (2007) The hypoxia-inducible factor alpha pathway couples angiogenesis to osteogenesis during skeletal development. *J Clin Invest* 117(6):1616–1626.
11. Rajicic N, et al.; Inflammation and the Host Response to Injury Large Scale Collaborative Research Program (2010) Identification and interpretation of longitudinal gene expression changes in trauma. *PLoS One* 5(12):e14380.
12. Desai KH, et al.; Inflammation and the Host Response to Injury Large-Scale Collaborative Research Program (2011) Dissecting inflammatory complications in critically injured patients by within-patient gene expression changes: A longitudinal clinical genomics study. *PLoS Med* 8(9):e1001093.

13. Albina JE, et al. (2001) HIF-1 expression in healing wounds: HIF-1alpha induction in primary inflammatory cells by TNF-alpha. *Am J Physiol Cell Physiol* 281(6): C1971–C1977.
14. Agarwal S, et al. (2015) BMP signaling mediated by constitutively active Activin type 1 receptor (ACVR1) results in ectopic bone formation localized to distal extremity joints. *Dev Biol* 400(2):202–209.
15. Zhao T, et al. (2015) Inhibition of HIF-1α by PX-478 enhances the anti-tumor effect of gemcitabine by inducing immunogenic cell death in pancreatic ductal adenocarcinoma. *Oncotarget* 6(4):2250–2262.
16. Zhang H, et al. (2008) Digoxin and other cardiac glycosides inhibit HIF-1alpha synthesis and block tumor growth. *Proc Natl Acad Sci USA* 105(50):19579–19586.
17. Ataliotis P (2000) Platelet-derived growth factor A modulates limb chondrogenesis both in vivo and in vitro. *Mech Dev* 94(1-2):13–24.
18. Orr-Urtreger A, Lonai P (1992) Platelet-derived growth factor-A and its receptor are expressed in separate, but adjacent cell layers of the mouse embryo. *Development* 115(4):1045–1058.
19. Uezumi A, et al. (2014) Identification and characterization of PDGFRα+ mesenchymal progenitors in human skeletal muscle. *Cell Death Dis* 5:e1186.
20. Downey J, et al. (2015) Prospective heterotopic ossification progenitors in adult human skeletal muscle. *Bone* 71:164–170.
21. Levi B, et al. (2015) Risk factors for the development of heterotopic ossification in seriously burned adults: A National Institute on Disability, Independent Living and Rehabilitation Research burn model system database analysis. *J Trauma Acute Care Surg* 79(5):870–876.
22. Lu MF, et al. (1999) Paired-related homeobox genes cooperate in handplate and hindlimb zeugopod morphogenesis. *Dev Biol* 205(1):145–157.
23. Barna M, Pandolfi PP, Niswander L (2005) Gli3 and Plzf cooperate in proximal limb patterning at early stages of limb development. *Nature* 436(7048):277–281.
24. Flannigan KL, et al. (2015) Proresolution effects of hydrogen sulfide during colitis are mediated through hypoxia-inducible factor-1α. *FASEB J* 29(4):1591–1602.
25. Lee K, Kim HM (2011) A novel approach to cancer therapy using PX-478 as a HIF-1α inhibitor. *Arch Pharm Res* 34(10):1583–1585.
26. Jacoby JJ, et al. (2010) Treatment with HIF-1alpha antagonist PX-478 inhibits progression and spread of orthotopic human small cell lung cancer and lung adenocarcinoma in mice. *J Thorac Oncol*5(7):940–949(2010).
27. Schwartz DL, et al. (2009) The selective hypoxia inducible factor-1 inhibitor PX-478 provides in vivo radiosensitization through tumor stromal effects. *Mol Cancer Ther* 8(4):947–958.
28. Koh MY, et al. (2008) Molecular mechanisms for the activity of PX-478, an antitumor inhibitor of the hypoxia-inducible factor-1alpha. *Mol Cancer Ther* 7(1):90–100.
29. Wang Y, Lei F, Rong W, Zeng Q, Sun W (2015) Positive feedback between oncogenic KRAS and HIF-1α confers drug resistance in colorectal cancer. *Onco Targets Ther* 8: 1229–1237.
30. Schwartz DL, et al. (2010) Radiosensitization and stromal imaging response correlates for the HIF-1 inhibitor PX-478 given with or without chemotherapy in pancreatic cancer. *Mol Cancer Ther* 9(7):2057–2067.
31. Sun K, Halberg N, Khan M, Magalang UJ, Scherer PE (2013) Selective inhibition of hypoxia-inducible factor 1α ameliorates adipose tissue dysfunction. *Mol Cell Biol* 33(5):904–917.
32. Bilbija D, et al. (2012) Retinoic acid signalling is activated in the postischemic heart and may influence remodelling. *PLoS One* 7(9):e44740.
33. Land SC, Tee AR (2007) Hypoxia-inducible factor 1alpha is regulated by the mammalian target of rapamycin (mTOR) via an mTOR signaling motif. *J Biol Chem* 282(28): 20534–20543.
34. Lin L, et al. (2011) Synergistic inhibition of endochondral bone formation by silencing Hif1α and Runx2 in trauma-induced heterotopic ossification. *Mol Ther* 19(8): 1426–1432.
35. National Research Council (2011) *Guide for the Use and Care of Laboratory Animals, Eighth Ed.* (National Academies, Washington, DC).
36. Cobb JP, et al.; Inflammation and Host Response to Injury Large-Scale Collaborative Research Program (2005) Application of genome-wide expression analysis to human health and disease. *Proc Natl Acad Sci USA* 102(13):4801–4806.
37. Calvano SE, et al.; Inflamm and Host Response to Injury Large Scale Collab. Res. Program (2005) A network-based analysis of systemic inflammation in humans. *Nature* 437(7061):1032–1037.

Supporting Information

Agarwal et al. 10.1073/pnas.1515397113

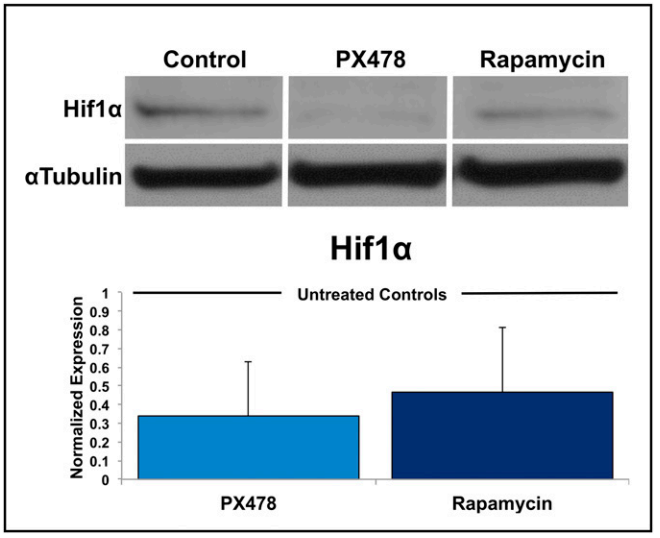

Fig. S1. PX-478 and rapamycin significantly decrease Hif1α protein production by mesenchymal cells isolated from uninjured tendon when cultured in hypoxia (n = 3 biological replicates for each treatment).

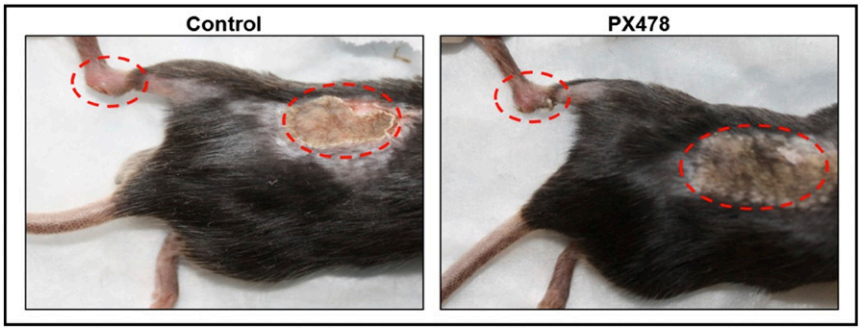

Fig. S2. Comparable healing of burn site and leg incision in PX-478– and control-treated burn/tenotomy mice 10 d after injury.

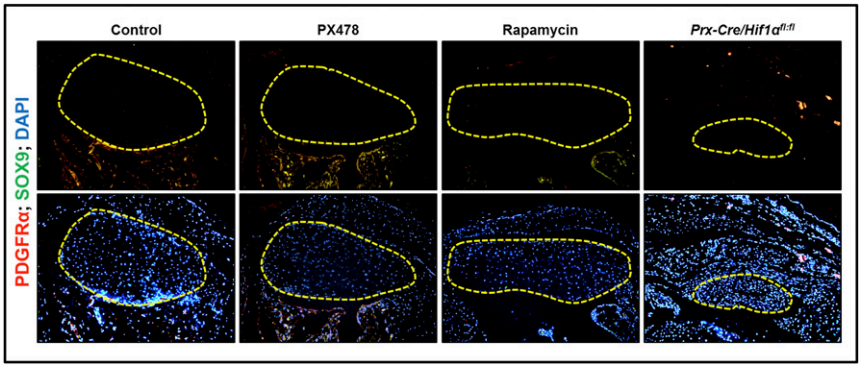

Fig. S3. Absence of PDGFRα^{+}/Sox9^{+} cells in the contralateral, uninjured tendon-calcaneal insertion (enthesis) of untreated, PX-478– or rapamycin-treated, or Cre-conditional Hif1α knockout mice. (Magnification: 20×.)

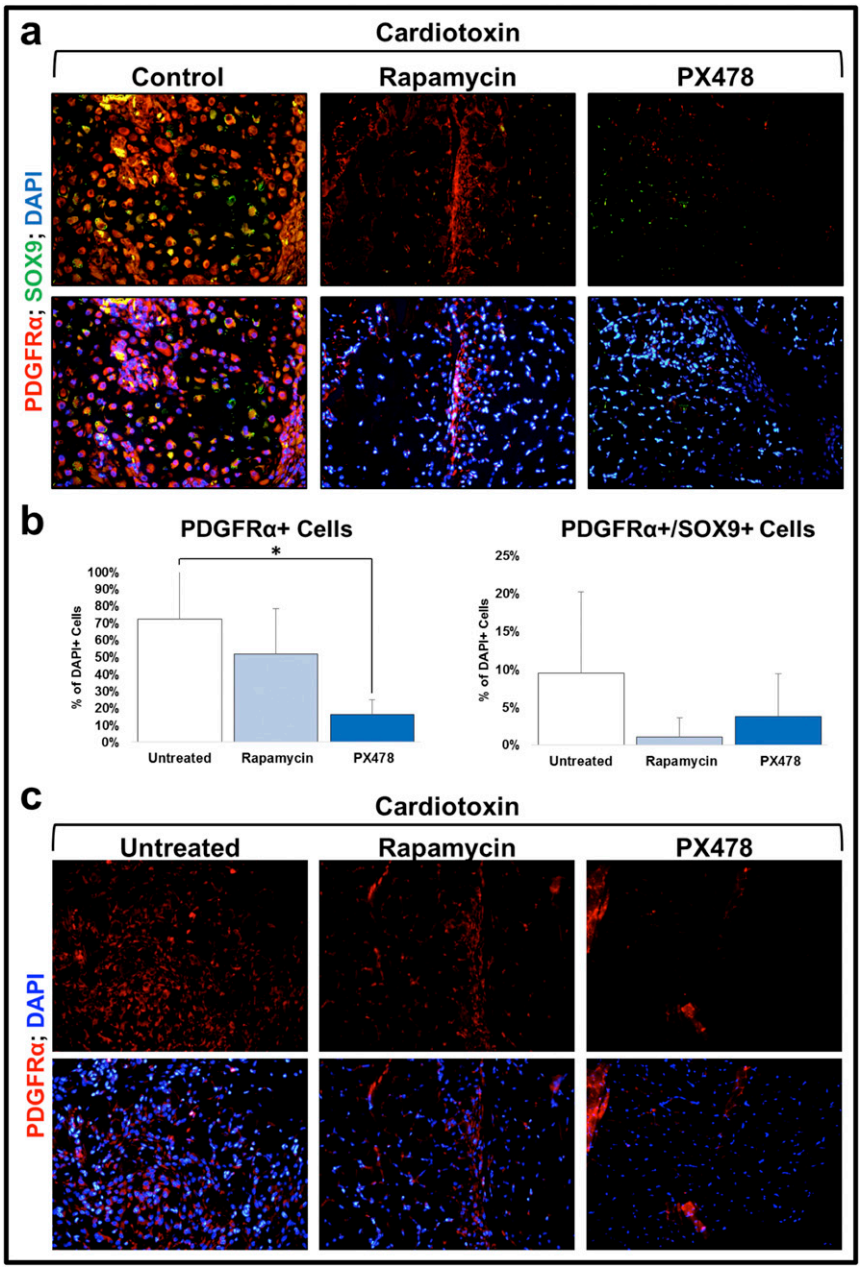

Fig. S4. Decreased mesenchymal progenitor cells and mesenchymal condensations in treated Ad.cre/cardiotoxin model. (*A*) Decreased PDGFRα$^+$/Sox9$^+$ condensing mesenchymal cells in PX-478– or rapamycin-treated mice 15 d after injury. (*B*) Quantification of PDGFRα$^+$ and PDGFRα$^+$/Sox9$^+$ cells in untreated, or PX-478– or rapamycin-treated mice 15 d after injury. (*C*) Decreased PDGFRα$^+$ mesenchymal progenitor cells in PX-478– or rapamycin-treated mice 5 d after injury. *$P < 0.05$. (Magnification: 20×.)

Table S1. Quantitative PCR primers

Species	Name	Accession no.	Primers (5′-3′)
Mouse	Hif1α	NM_176958	F-GTCCCAGCTACGAAGTTACAGC
			R-CAGTGCAGGATACACAAGGTTT
	Sox9	NM_011448	F-AGTACCCGCATCTGCACAAC
			R-ACGAAGGGTCTCTTCTCGCT
	Acan	NM_007424	F-ACTGCGACATCTGGAGTGAC
			R-CTGTCCACTGCCAAAGAGAA